ChemPubSoc Europe

DOI: 10.1002/cssc.201900779

CHEMSUSCHEM Full Papers

Unveiling Electrochemical Reaction Pathways of CO_2 Reduction to C_N Species at S-Vacancies of MoS_2

Sungwoo Kang,[a] Seungwu Han,[a] and Youngho Kang*[b]

Although C_1 species such as CO and CH_4 constitute the majority of CO_2 reduction (CO_2R) products on known catalysts, recent experiments showed that 1-propanol with two C–C bonds is produced as the main CO_2R product on MoS_2 single crystals in aqueous electrolytes. Herein, the CO_2R mechanism on MoS_2 is investigated by using first-principle calculations. Focusing on S-vacancies (V_S) as the catalytic site, potential free-energy pathways to various CO_2R products are obtained by means of a computational hydrogen electrode model. The results underline the role of HCHO, which is one of the elemental C_1 products, in opening pathways to C_N species for $N>1$. Key steps to increase C–C bonds are the adsorption of HCHO at the V_S site and binding of another HCHO to the adsorbed one. The predicted products and theoretical working potentials to open their pathways are consistent with experiments, which indicates that V_S is an important active site for CO_2R on the MoS_2 basal plane.

Introduction

The electrochemical conversion of CO_2 into carbon-neutral fuels is a promising avenue toward simultaneously resolving two challenges for a sustainable society, that is, the surging energy demand and extreme climate change. In CO_2 conversion, the catalyst is a prime component, and there have been extensive efforts to develop catalysts for electrochemical CO_2 reduction (CO_2R) that possess both high efficiency and good selectivity.[1,2] Transition metals such as Cu, Au, Pd, and their alloys have been the subject of numerous researches for CO_2R.[3–8] On most metal electrodes, the primary products of CO_2R are carbon monoxide (CO) and formic acid (HCOOH). Only Cu yields various carbon species ranging from single-carbon molecules such as CO, methane (CH_4), and methanol (CH_3OH) to multi-carbon species such as ethylene (C_2H_4) and ethanol (CH_3CH_2OH).[7,8] However, the large overpotential [≈ -1 V vs. reversible hydrogen electrode (RHE)] and low selectivity of Cu for CO_2R impede its practical utilization.

MoS_2 catalysts have received tremendous attention for electrochemical reduction of chemicals owing to their high durability in reducing conditions, earth abundance, and two-dimensional nature.[9–16] Although the outstanding catalytic performance of MoS_2 in producing hydrogen from water has been confirmed in numerous studies over the past several years, its activity for CO_2R has attracted attention only recently; experiments have demonstrated that MoS_2 exhibits high Faradaic efficiency (FE) and good selectivity to CO in ionic liquids with Mo edges as the active sites.[17–19] Recently, Francis et al. investigated CO_2R on single-crystal MoS_2 in aqueous electrolyte, discovering 1-propanol ($CH_3CH_2CH_2OH$) as a major CO_2R product at moderate overpotentials (≈ -0.59 V vs. RHE), although the CO_2R efficiency was still outperformed by the hydrogen evolution reaction (HER).[20] This result is surprising because C_3 species are rarely produced as a major product of CO_2R on known catalysts, particularly at such small overpotentials. The only exception that we are aware of are nickel phosphides, which were recently reported to generate methylglyoxal (CH_3COCHO) and ring-shaped 2,3-furandiol ($C_4H_4O_3$) as major products.[21] In this respect, the catalytic behavior of MoS_2 for CO_2R is unique. To identify the active site of MoS_2, Francis et al. measured FE while changing the edge density of MoS_2 and found that the FE of the 1-propanol production decreased with increasing edge density.[20] This implies that the active site is likely to be present at the basal plane rather than the edges. However, the clean surface of MoS_2 is known to be inert,[22] and thus, the nature of the active site responsible for CO_2R to 1-propanol is still elusive.

In this work, we investigate the electrochemical pathways of CO_2R on MoS_2 to various products including multi-carbon species by using ab initio calculations. As a potential active site for CO_2R on the MoS_2 basal plane, we pay attention to S-vacancies (V_S), which are also known to be a catalytic site for HER.[23–25] It is noted that sizable concentrations ($\approx 10\%$)[25] of V_S can occur during the fabrication of MoS_2 films, and V_S are theoretically predicted to have low formation energy (1–3 eV depending on the growth conditions).[26,27] To illustrate how V_S can catalyze the CO_2R reaction, we adopt a computational hydrogen electrode (CHE) model,[28] which is modified to reflect the fact that

[a] S. Kang, Prof. Dr. S. Han
Department of Materials Science and Engineering
Seoul National University
Seoul 08826 (Republic of Korea)

[b] Dr. Y. Kang
Materials Data Center
Korea Institute of Materials Science
Changwon 51508 (Republic of Korea)
E-mail: thehoya84@gmail.com

Supporting Information and the ORCID identification number(s) for the author(s) of this article can be found under: https://doi.org/10.1002/cssc.201900779.

V_S in semiconducting MoS_2 can trap charge carriers. We show that the bowl shape of V_S leads to the formation of *OCHO rather than *COOH at the initial protonation step (* denotes the vacancy site or adsorbed species). Starting from *OCHO, we suggest thermodynamically favorable pathways leading to various C_N species ($N=1$–3). Our results highlight the role of formaldehyde (HCHO), which is one of the elementary C_1 products likely to be produced at V_S, for opening pathways to C_2 and C_3 species. The key steps to increase C–C bonds are the adsorption of HCHO at the vacancy site and binding of the next HCHO to the adsorbed one. The predicted overpotentials to open C_N species are in good agreement with experiments, supporting that V_S is the key active site for CO_2R, which produces 1-propanol.

Results and Discussion

Charge states of sulfur vacancies

Figure 1 shows the density of states (DOS) of V_S-MoS_2. Three sub-gap states associated with V_S were identified: a singlet a_1 and doubly degenerated e states.[27] These states were highly localized at the neighboring Mo sites, as can be seen in the charge density distributions of the corresponding electronic states (see figures on the top of Figure 1). In the neutral state, the a_1 state was fully occupied whereas the e states were empty. Consequently, including the spin degree of freedom, the local charge state of V_S could vary between −4 and +2 (+ and − indicate removal and addition of electrons, respectively). It is generally assumed that electron and proton transfer occur concurrently during the reduction process on heterogeneous catalysts.[28] This assumption would be valid for conventional metallic catalysts, in which electronic wave functions are delocalized over numerous atomic sites and the localization of electrons around the active site requires an incoming proton.[29] In contrast, the sub-gap states associated with V_S in MoS_2 are inherently localized and, therefore, the two processes can occur independently.[30]

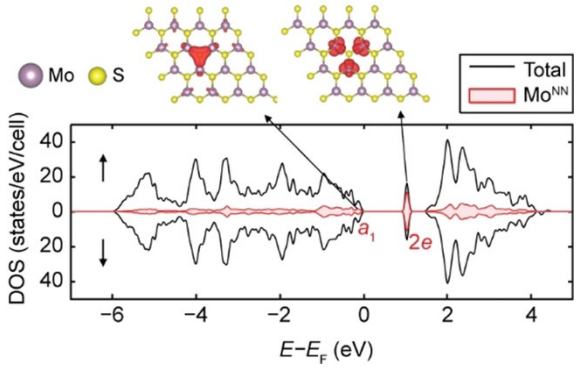

Figure 1. Spin-resolved total DOS of V_S-MoS_2. Partial DOS projected on three nearest-neighbor Mo ions (Mo^{NN}) near V_S are present in red. Partial charge densities corresponding to the vacancy states (a_1 and $2e$ states) are provided.

The range of charge states in the active site, either bare V_S or adsorbed intermediate, depends on intermediates owing to the electronic coupling between the vacancy and adsorbates.[22] For instance, *OCHO and *OH shifted down the a_1 state into the valence band whereas the e states remained within the band gap (see Figure S1 a, b in the Supporting Information). Because an electron from the adsorbates occupied one of the e levels in the neutral state, the possible charge state was from −3 to +1 for these intermediates. As another example, in the case of *O, no sub-gap states were identified (see Figure S1 c in the Supporting Information). Consequently, only the neutral state was considered.

CHE model for V_S-MoS_2

To calculate the free energy of each intermediate considering the RHE conditions, we employed the CHE model.[28] This model enables implicit simulation of electrochemical environments such as electrode potential and solvated protons by assuming that the chemical potentials of H^+ [$\mu(H^+)$] and e^- [$\mu(e^-)$] are determined by the chemical potential of H_2 [$\mu(H_2)$] and electrode potential (U) according to Equations (1) and (2):

$$\mu(H^+) + \mu_{RHE}(e^-) = \frac{1}{2}\mu(H_2) \quad (1)$$

$$\mu(e^-) = \mu_{RHE}(e^-) - eU = \mu_{SHE}(e^-) + 0.059\,pH - eU \quad (2)$$

in which e denotes the magnitude of electron charge (1.60×10^{-19} C), $\mu_{SHE}(e^-)$ is the electron chemical potential of the standard hydrogen electrode (SHE), which is −4.44 eV on the absolute scale, and U is the electrode potential with respect to RHE. By combining Equations (1) and (2), $\mu(H^+)$ is determined according to Equation (3):

$$\mu(H^+) = \frac{1}{2}\mu(H_2) + 4.44\,eV - 0.059\,pH \quad (3)$$

In metallic catalysts, the reaction step proceeds by adding a proton–electron pair to the former reactant. This means that the reaction free energy depends on U linearly,[28] but it is not affected by pH under the RHE conditions. This is not the case for V_S-MoS_2, in which the electron transfer is independent from the protonation step. Accordingly, the reaction free energy of a protonation step proceeding from the ith to the $(i+1)$th intermediate ($\Delta G_{i\to i+1}$) depends on potential U and pH according to Equation (4):

$$\Delta G_{i\to i+1} = G(M_{i+1}, q^U_{i+1}) - G(M_i, q^U_i) - \frac{1}{2}\mu(H_2) + eU \times (q^U_i - q^U_{i+1} + 1) - 0.059\,pH \times (q^U_i - q^U_{i+1}) \quad (4)$$

in which q_i^U is the most stable charge state of V_S for an ith intermediate M_i at the given U. Throughout this paper, U is referenced to RHE [V vs. RHE]. Because neutral solutions are typically used for electrochemical CO_2R,[31] the pH was set to be 7. To determine q_i^U, we first checked the availability of sub-gap states for M_i and evaluated the charging energy of M_i for all of

possible charge states q, that is, $G(M_i,q)-G(M_i,0)-q\times eU$. Then, we selected the q leading to the lowest charging energy at a given U as q_i^U.[30] If the charge state is the same between successive intermediates, that is, $q_i^U-q_{i+1}^U=0$, $\Delta G_{i\to i+1}$ linearly depends on U, as found in metallic catalysts. Equation (4) indicates that a decrease of the charge state after a hydrogenation, namely taking more electrons from RHE, lowers $\Delta G_{i\to i+1}$ at negative potentials compared with the case of $q_i^U=q_{i+1}^U$. Conversely, a rise in the charge state increases $\Delta G_{i\to i+1}$. As a consequence, $\Delta G_{i\to i+1}$ along a reaction pathway on V_S-MoS_2 may not monotonically decrease with increasingly negative potentials.

The catalytic performance of CO_2R reactions was compared in terms of the theoretical working potential (η_{theory}), which is defined as the least-negative potential at which the ΔG for the potential-limiting step becomes negative. It has been found that η_{theory} correlates well with the experimental onset potential.[32,33] We noted that the ΔG for the initial protonation step that exists in every pathway was always positive (see Figure S2 in the Supporting Information) regardless of U because it did not involve electron transfer from the electrode. However, the ΔG of this first protonation step was not so high ($\approx$0.3 eV).[34] In addition, the highest ΔG at zero bias occurred at another step in the reaction pathway, except for the formation of HCOOH (see below). Thus, assuming that the first protonation step is not critical for opening pathways for CO_2R (but this could be a crucial factor to determine the selectivity of the CO_2R reaction against HER, which will be discussed later), we determined η_{theory} by the downhill condition of the free energy after the formation of *OCHO and considered it as an estimator for the experimental onset potential.

Pathways to elementary C_1 products

There are numerous potential pathways for CO_2R reactions. To find out the lowest-energy pathway to C_1 products, we first examined reaction pathways that were proposed to investigate the CO_2R reactions on Cu.[35] In addition to the suggested possible pathways, we also tested other probable pathways by thoroughly considering geometry and chemical characteristics of adsorbates. Throughout this work, we assumed that intermediates readily accomplished their stable charge state prior to further protonation because the electron transfer was much faster than the proton transfer on the electrode. Therefore, reaction pathways were described only with respect to the total number of transferred protons [n(H)] (see Figures 2, 3, and 5–7).

We present the lowest-energy pathway to formic acid in Figure 2a. We set the zero energy for C_1 pathways as the calculated free energy of a system that consisted of V_S-MoS_2 and one CO_2 molecule. The integer number at each intermediate in the free-energy diagram indicates the stable charge state of the corresponding active site. It is intriguing to note that, in contrast to transition-metal surfaces, for which the initial protonation step of CO_2 produces *COOH,[36] the first protonation product at V_S of MoS_2 was *OCHO, which is lower in energy by 0.84 eV than *COOH (the detailed reaction pathway starting with *COOH to CH_4 is compared to one with *OCHO in Figure S3 in the Supporting Information). The difference in the free energy between *OCHO and *COOH was attributed to the bowl shape of V_S, which sterically hindered incorporation of two atoms into the vacancy site.[37]

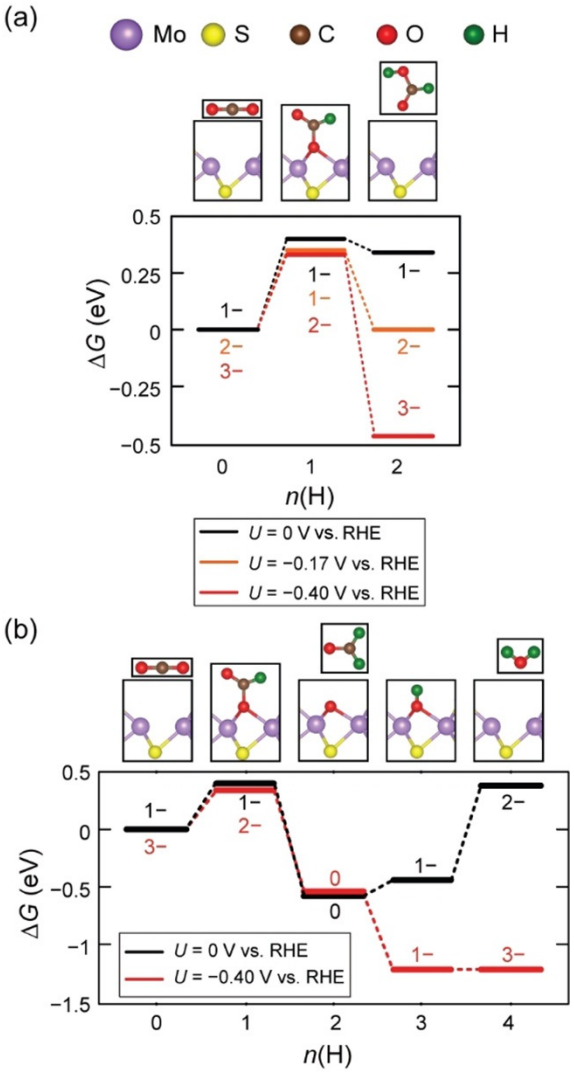

Figure 2. Free-energy diagrams for the lowest-energy pathways to (a) HCOOH and (b) HCHO. The integer number at each intermediate indicates the stable charge state of V_S at the given potentials.

The highest free-energy step in the pathway to formic acid was the formation of *OCHO, with $\Delta G=0.33$ eV at 0 V. As mentioned above, this did not vanish at negative potentials. However, ΔG in the second protonation step gradually decreased with potential and vanished at −0.17 V (Figure 2a). Further decrease of potential made the overall HCOOH pathway exergonic. Therefore, this pathway may open at −0.17 V.

Figure 2b shows the reaction pathway to formaldehyde. The fourth reduction step to generate H_2O yielded the maximum ΔG of 0.82 eV at 0 V, which was owing to the strong Mo–O bonding.[38] The ΔG became zero at −0.40 V, that is, $\eta_{theory}=-0.40$ V, rendering every reaction step downhill after *OCHO. It is noteworthy that the magnitude of η_{theory} for the formation of

HCHO was smaller than ΔG to form H_2O at 0 V (0.82 eV) because this reaction involved lowering the charge state. Between formic acid and formaldehyde, the latter was expected to evolve more efficiently because the free energy of the second protonation step, which determines the selectivity, was more exergonic in the pathway to HCHO than HCOOH.[39]

Pathways to C_N products involving the adsorption of HCHO at V_S

Because HCOOH and HCHO are highly soluble in water and reactive, they are likely to be further reduced to other species instead of being released to the outside of solutions.[21,35,40,41] Between them, we focused on pathways led by the adsorption of HCHO because its formation would dominate that of HCOOH, as stated above. In addition, HCHO was bound to V_S more strongly than HCOOH; the binding constant of HCHO at V_S was calculated to be 2.8×10^{-6} L mol^{-1}, which was even higher than 2.5×10^{-11} L mol^{-1} for HCOOH.

The additional protonation of *HCHO led to the formation of *OCH_3, followed by the production of CH_4, as shown in Figure 3a. Like for HCHO formation, ΔG reached the maximum when *OH was reduced to H_2O at 0 V, leading to −0.40 V for η_{theory}. HCHO could also be added to the *O that was left after the second protonation step of *OCHO. Then, the proton transfer to *OCH_2O generated *OCH_2OH and eventually CH_3OH, as shown in Figure 3b. In this case, the third protonation step to form *OCH_2OH caused the maximum ΔG of 1.00 eV at 0 V. However, this ΔG decreased more rapidly with potential than for the formation of H_2O owing to the larger difference in the charge state between the successive intermediates. As a result,

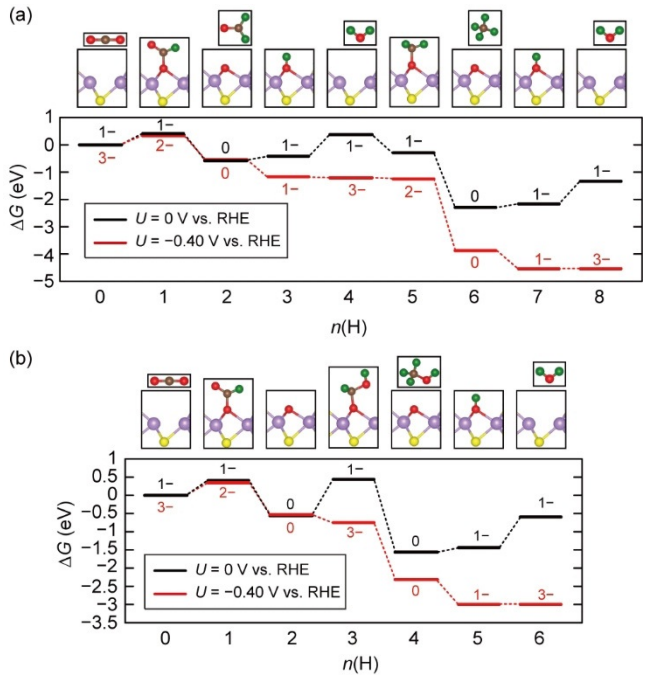

Figure 3. Free-energy diagrams for the lowest-energy pathways to (a) CH_4 and (b) CH_3OH. The integer number at each intermediate indicates the stable charge state of V_S at the given potentials.

η_{theory} for the pathway to CH_3OH was −0.40 V, which was the same as that for CH_4.

We then turned to the discussion of potential pathways to C_2 products. Previously, the dimerization between intermediates containing sp or sp^2 carbon atoms such as *CO or *COH was proposed as a key step to create a C–C bond.[34–36,42,43] This mechanism is feasible on metal catalysts, on which surface adsorbates can approach each other through diffusion. However, this is unlikely to happen in V_S-MoS_2. Instead, *OCHO and *HCHO can become a source to make a C–C bond through the direct interaction with dissolved HCHO or CO_2 molecules, as depicted in Figure 4. These reactions are expected to occur more readily at V_S than on metal surfaces because the sp^2 carbon atoms in *OCHO and *HCHO are exposed to electrolyte.

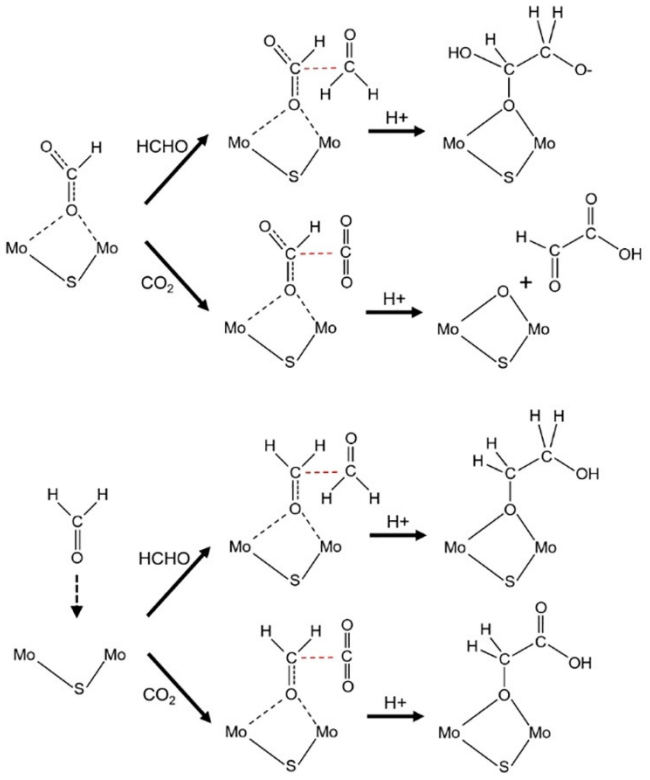

Figure 4. Possible reactions to create a C–C bond at V_S during CO_2R reaction. The red dashed lines indicate the formation of a C–C bond through the direct coupling between adsorbates and dissolved molecules.

Among the possible reactions presented in Figure 4, we found that the reaction between *HCHO and HCHO was energetically most favorable in forming the C–C bond. To be specific, the reaction free energies of *OCHO + HCHO + $H^+\rightarrow$ *$OCHOHCH_2O$ and *OCHO + CO_2 + $H^+\rightarrow$ *O + HCOOH were 1.70 and 0.27 eV at −0.40 V, respectively, and these free energies did not decrease to zero by applying overpotentials down to −1 V. In contrast, *HCHO + HCHO + $H^+\rightarrow$ *OCH_2COOH resulted in negative reaction free energies at overpotentials between −1 and 0 V. Furthermore, the reactions involving *OCHO to create a C–C bond competed with the one produc-

ing HCHO, namely $*OCHO + H^+ \rightarrow *O + HCHO$, but the latter was expected to occur dominantly owing to the smaller reaction free energy of −0.98 eV at −0.4 V compared with those of the former. Thus, *OCHO primarily led to the production of HCHO, but not multi-carbon species. The HCHO condensation competed with $*HCHO + CO_2 + H^+ \rightarrow *OCH_2COOH$, but the latter yielded the higher reaction free energy (for the C_2 pathway led by the adsorption of CO_2 to *HCHO, see Figure S4 in the Supporting Information). The condensation of HCHO molecules was also suggested as a key process, increasing C–C coupling at nickel phosphide electrodes.[21] Below, we analyzed in detail the C_2 pathways proceeding through the HCHO condensation.

There are two potential C_2 species: ethylene glycol ($HOCH_2CH_2OH$) and ethanol, to which the pathways are shown in Figure 5a,b, respectively. For a concise representation of pathways to C_N products with $N \geq 2$, we adjusted the zero energy in free-energy diagrams to the one of V_S-MoS_2 + N(HCHO) with the stable charge state and omitted the protonation steps to produce N(HCHO). We found that the protonation steps of HCHO to produce ethylene glycol were exergonic. As a result, the reaction of $*OH + H^+ \rightarrow H_2O$ to produce HCHO would yield the highest ΔG for this CO_2R reaction, predicting this pathway to open at −0.40 V. Similarly, the reaction $2\,HCHO + 2\,H^+ \rightarrow CH_3CH_2OH + *O$ was downhill in energy. Therefore, the same η_{theory} (−0.40 V) was obtained for the pathway to ethanol.

We also examined C_N pathways for $N \geq 3$ proceeding through the condensation of HCHO molecules at V_S. Figure 6a,b shows the reaction pathways to 1,3-propanediol ($HOCH_2CH_2CH_2OH$) and 1-propanol, respectively. These pathways were found to open at −0.40 V. The ΔG of the alcohol substitution reaction of the C_4 pathway remained positive (0.47 eV) at −0.40 V because of the increase in the charge state (see Figure S5 in the Supporting Information). This positive reaction energy diminished but did not completely vanish at more negative potentials down to −1 V, implying that pathways to C_4 species are more difficult to open compared with other C_N products for $N < 4$.

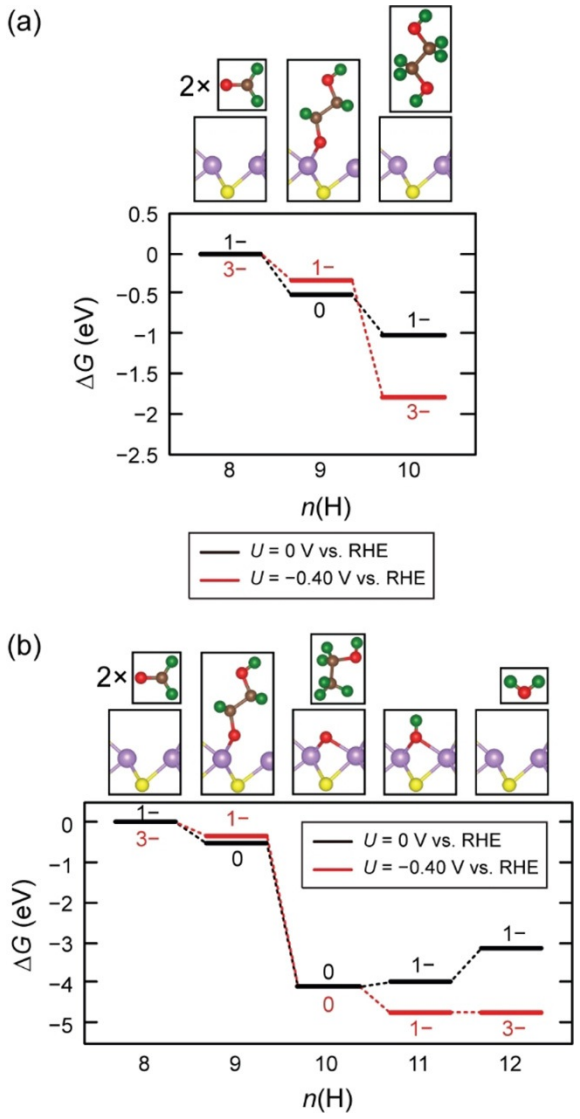

Figure 5. Free-energy diagrams for the lowest-energy pathways to (a) $HOCH_2CH_2OH$ and (b) CH_3CH_2OH. The integer number at each intermediate indicates the stable charge state of V_S at the given potentials.

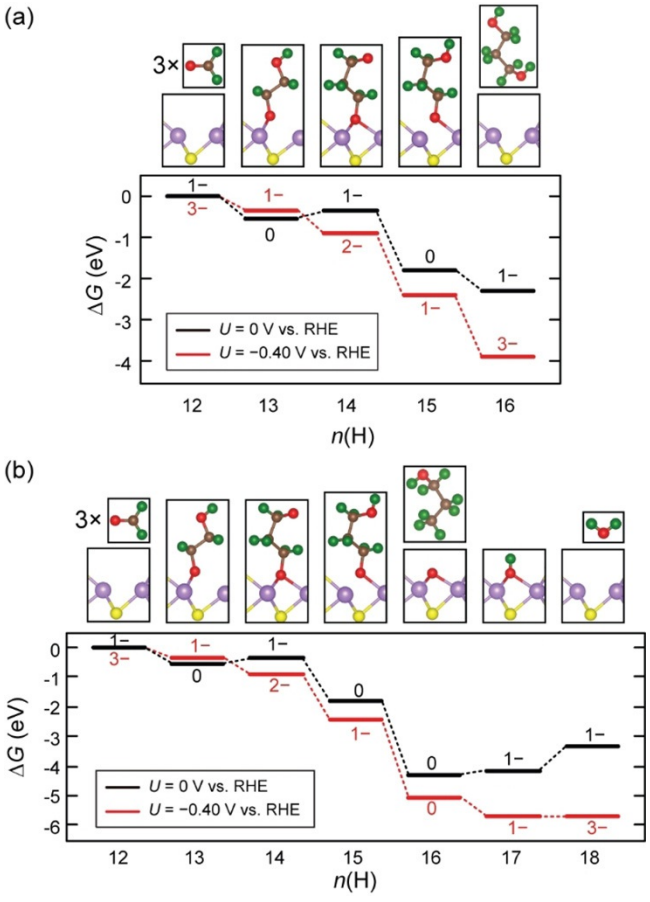

Figure 6. Free-energy diagrams for the lowest-energy pathways to (a) $HOCH_2CH_2CH_2OH$ and (b) $CH_3CH_2CH_2OH$. The integer number at each intermediate indicates the stable charge state of V_S at the given potentials.

Comparison with experiments

In the previous section, we showed that multiple pathways starting from the adsorption of HCHO could open at −0.40 V. This value of η_{theory} is consistent with the onset potential between −0.59 and −0.50 V in experiments associated with the formation of 1-propanol, the major CO_2R product, but also ethylene glycol.[20] We note that the pH in the experiments was 6.8, which is slightly smaller than 7.0 in our calculations. This pH difference changed the η_{theory} by approximately 0.01 V, barely affecting our conclusion.

Our CHE model also suggested that opening the route to the formation of C_N species for $N>3$ is difficult. In fact, C_4 species such as 1-butanol and 1,4-butanediol, which are potential products from the HCHO condensation, were not detected in experiments. This favorable comparison of computational results with experiments illustrates that V_S serves as the important active site for CO_2R.

We also tried to determine the C_N product with the highest selectivity within the CHE framework. To this end, we compared the reaction free energies between competing reactions following the pathways to C_3 products when a protonation could produce different intermediates. Then, we kept track of the lowest-energy pathway.[35,39,44] The analysis of all reaction pathways revealed that the route to ethanol was most favorable, followed by ethylene glycol and 1-propanol (see Figure S6 in the Supporting Information). However, ethanol was not detected in the experiment. According to previous work,[35,39] it is reasonable to identify the main CO_2R products based on reaction free energies at given overpotentials if the reaction pathways purely consist of simple protonation steps, even if reaction barriers can still come into play. The situation, however, becomes more complicated in the case of reaction pathways to multi-carbon species, which involves reactions for the C–C bond formation in addition to the protonation. As a result, comparing reaction free energies between competing reactions would be insufficient for judging the relative selectivity among potential products. We believe that to fully resolve this inconsistency between experimental and predicted products, a further kinetic study associated with competing reactions during the formation of ethanol and 1-propanol is needed, which will be the subject of future work.

Selectivity of CO_2R versus HER

Despite clear advantages of V_S-MoS_2 for CO_2R, such as the multi-carbonated products (1-propanol)[45] and low onset potential (−0.5 V), this catalyst still suffers from the lower selectivity against HER.[20] This can be qualitatively understood by the difference in reaction free energies of competing reactions between HER and CO_2R. For comparison with the CO_2R pathway, we present the HER pathway in Figure 7. It is clear that the HER pathway is expected to be favored over that for the CO_2R because $\Delta G(*H)-\Delta G(*OCHO)$ is −0.66 eV at −0.4 V. However, the pathway to 1-propanol can compete with HER if the reaction starts with formaldehyde rather than CO_2, resulting in $\Delta G(*H)-\Delta G(*OCH_2CH_2OH)=-0.01$ eV at −0.4 V. Therefore, cascade catalysts[46–48] combining V_S-MoS_2 and other catalysts, which can produce formaldehyde efficiently as a CO_2R product, such as polyhydride ruthenium complexes, boron-doped diamond, and Cu,[41,49,50] may offer improved selectivity for 1-propanol production.

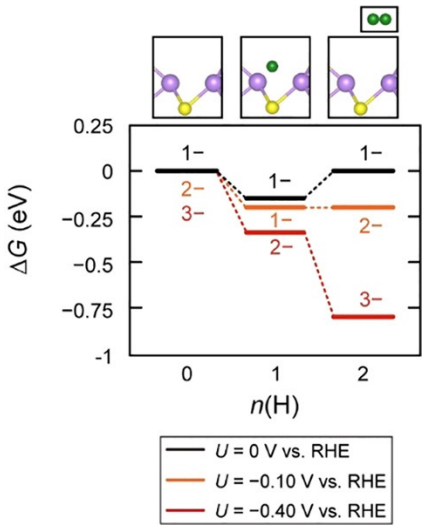

Figure 7. Free-energy diagrams for the lowest-energy pathways to H_2. The integer number at each intermediate indicates the stable charge state of V_S at the given potentials.

Doping would also be another strategy to resolve the selectivity issue, as demonstrated for MoS_2 edges by Hong et al.[51] By using the CHE model, they showed that the catalytic activity of CO_2R and its selectivity over HER on pure MoS_2 edges are not favorable but can be improved by the incorporation of transition metals. For facilitating CO_2R to multi-carbon species at the S-vacancy of the basal plane, metal dopants enabling both the efficient formation of V_S and the stabilization of *OCHO will be advantageous.

Conclusions

We theoretically analyzed possible electrochemical pathways for electrochemical CO_2 reduction (CO_2R) on V_S-MoS_2 (V_S=S-vacancies) by means of the modified computational hydrogen electrode (CHE) model. We showed that the condensation of HCHO molecules is a key to allow C–C coupling at V_S. The CHE model predicts that pathways to multiple C_N species for $N<4$ can open at −0.40 V whereas the formation of C_4 products is unfavored at such low potentials. These results are in reasonable agreement with recent experiments, indicating that V_S of MoS_2 serves as the important active site for CO_2R. We also discussed the ways to overcome the poor selectivity of CO_2R against the hydrogen evolution reaction: cascade catalysts and doping. By unveiling the nature of the active site and mechanisms of CO_2R to multi-carbon species at V_S-MoS_2, this study will contribute to designing catalysts to produce hydrocarbon fuels with high energy densities.

Computational Setup

The ab initio calculations were performed with the Vienna ab initio simulation package (VASP).[52] The Perdew–Burke–Ernzerhof (PBE) functional was used for describing exchange-correlation potentials.[53] The plane-wave cutoff energy was set to 450 eV. To simulate V_S-MoS_2, one S atom was removed from a 4×4 MoS_2 supercell. A vacuum with approximately 15 Å thickness was incorporated in the supercells to avoid interactions between repeated images along the vertical direction within the periodic boundary condition. The 7×7×1 and 3×3×1 Monkhorst–Pack meshes were used for the unit cell and supercell, respectively. All atomic structures were fully relaxed until all directional components of the atomic force acting on each atom were reduced to below 0.02 eV Å^{-1}. Grimme's D2 scheme was employed to account for van-der-Waals interactions.[54] The change of van-der-Waals functional barely affected our conclusions (see Table S1 in the Supporting Information). Effects of solvation were taken into account by the implicit solvation model, which approximates solvent molecules with a dielectric continuum[55] with parameters of 78.4 (dielectric constant), 0.6 Å (cavity width), 0.525 meV Å^{-2} (surface tension), and 0.0025 Å^{-3} (cutoff density). These parameters were reported to accurately reproduce the experimental solvation energies of a water molecule and hydronium ion in the literature.[30] The vibrational entropy and zero-point energies were considered in the free energy of adsorbed intermediates within the harmonic approximations.[56] For gas phases, experimental entropies were used to calculate the free energy, taking all degree of freedoms (translation, rotation, and vibration) into account.[57] We assumed that the partial pressure of all gas phases was 1 atm for the simplicity of computations, but its variation (from 0.01 to 1 atm) had a minor effect on the free energy of systems less than 0.12 eV. The free energy of a H_2O molecule in aqueous electrolyte was calculated by assuming the equilibrium with its gas phase at room temperature, as in previous works.[35] For the calculations of charged systems, we did not consider corrections to the total energy because they were reported to be negligible owing to the high dielectric constant of water.[30] Indeed, we found that the Markov and Payne scheme, which had been modified for two-dimensional systems in Ref. [27], resulted in an increase of the total energy of V_S with the 3− charge state just by 0.12 eV considering the dielectric constant of water. The magnitude of the correction was proportional to the square of the charge state, and therefore a correction to the total energy of other charge states, that is, 2−, 1−, and 1+, should be smaller. The influence of this correction to the total energy of $V_S(3-)$ on the theoretical working potential was weaker; the overpotential to render the reaction free energy of $*OH(1-)+H^+ \rightarrow V_S(3-)+H_2O$, a potential limiting step for the majority of the CO_2R products including 1-propanol, to be zero only negatively increased by 0.04 V, which was nearly one-third of the correction for $V_S(3-)$ owing to the reduction of the charge states during this protonation step. Accordingly, our conclusion was not affected by the energy correction for charged systems. We provided CONTCAR files, which include the geometry information of supercells, and corresponding DFT energies for every intermediate used to produce all pathways considered in the present work at 0 and −0.4 V, in the Supporting Information.

Acknowledgements

We thank Prof. Jihun Oh for helpful discussions. This work was supported by the Creative Materials Discovery Program through the National Research Foundation of Korea (NRF) funded by the Ministry of Science and ICT (2017M3D1A1040689). The computation was carried out at the KISTI supercomputing center (grant no. KSC-2018-C3-0022). Y.K. acknowledges the Fundamental Research Program (No. PNK6410) of the Korea Institute of Materials Science, Republic of Korea.

Conflict of interest

The authors declare no conflict of interest.

Keywords: CO_2 reduction · density functional theory · electrocatalysis · MoS_2 · multicarbon species

[1] Y. Li, Q. Sun, *Adv. Energy Mater.* **2016**, *6*, 1600463.
[2] C. Costentin, M. Robert, J.-M. Savéant, *Chem. Soc. Rev.* **2013**, *42*, 2423.
[3] Y. Hori, H. Wakebe, T. Tsukamoto, O. Koga, *Electrochim. Acta* **1994**, *39*, 1833.
[4] B. A. Rosen, A. Salehi-Khojin, M. R. Thorson, W. Zhu, D. T. Whipple, P. J. A. Kenis, R. I. Masel, *Science* **2011**, *334*, 643.
[5] Y. Chen, C. W. Li, M. W. Kanan, *J. Am. Chem. Soc.* **2012**, *134*, 19969.
[6] H. Mistry, R. Reske, Z. Zeng, Z.-J. Zhao, J. Greeley, P. Strasser, B. R. Cuenya, *J. Am. Chem. Soc.* **2014**, *136*, 16473.
[7] S. Kaneco, H. Katsumata, T. Suzuki, K. Ohta, *Energy Fuels* **2006**, *20*, 409.
[8] A. S. Varela, W. Ju, T. Reier, P. Strasser, *ACS Catal.* **2016**, *6*, 2136.
[9] J. D. Benck, T. R. Hellstern, J. Kibsgaard, P. Chakthranont, T. F. Jaramillo, *ACS Catal.* **2014**, *4*, 3957.
[10] A. B. Laursen, S. Kegnæs, S. Dahl, I. Chorkendorff, *Energy Environ. Sci.* **2012**, *5*, 5577.
[11] D. Deng, K. S. Novoselov, Q. Fu, N. Zheng, Z. Tian, X. Bao, *Nat. Nanotechnol.* **2016**, *11*, 218.
[12] D. M. Andoshe, J. M. Jeon, S. Y. Kim, H. W. Jang, *Electron. Mater. Lett.* **2015**, *11*, 323.
[13] Y. Li, H. Wang, L. Xie, Y. Liang, G. Hong, H. Dai, *J. Am. Chem. Soc.* **2011**, *133*, 7296.
[14] B. Hinnemann, P. G. Moses, J. Bonde, K. P. Jørgensen, J. H. Nielsen, S. Horch, I. Chorkendorff, J. K. Nørskov, *J. Am. Chem. Soc.* **2005**, *127*, 5308.
[15] T. F. Jaramillo, K. P. Jorgensen, J. Bonde, J. H. Nielsen, S. Horch, I. Chorkendorff, *Science* **2007**, *317*, 100.
[16] D. Kong, H. Wang, J. J. Cha, M. Pasta, K. J. Koski, J. Yao, Y. Cui, *Nano Lett.* **2013**, *13*, 1341.
[17] M. Asadi, B. Kumar, A. Behranginia, B. A. Rosen, A. Baskin, N. Repnin, D. Pisasale, P. Phillips, W. Zhu, R. Haasch, R. F. Klie, P. Král, J. Abiade, A. Salehi-Khojin, *Nat. Commun.* **2014**, *5*, 4470.
[18] M. Asadi, K. Kim, C. Liu, A. V. Addepalli, P. Abbasi, P. Yasaei, P. Phillips, A. Behranginia, J. M. Cerrato, R. Haasch, P. Zapol, B. Kumar, R. F. Klie, J. Abiade, L. A. Curtiss, A. Salehi-Khojin, *Science* **2016**, *353*, 467.
[19] P. Abbasi, M. Asadi, C. Liu, S. Sharifi-Asl, B. Sayahpour, A. Behranginia, P. Zapol, R. Shahbazian-Yassar, L. A. Curtiss, A. Salehi-Khojin, *ACS Nano* **2017**, *11*, 453.
[20] S. A. Francis, J. M. Velazquez, I. M. Ferrer, D. A. Torelli, D. Guevarra, M. T. McDowell, K. Sun, X. Zhou, F. H. Saadi, J. John, M. H. Richter, F. P. Hyler, K. M. Papadantonakis, B. S. Brunschwig, N. S. Lewis, *Chem. Mater.* **2018**, *30*, 4902.

[21] K. U. D. Calvinho, A. B. Laursen, K. M. K. Yap, T. A. Goetjen, S. Hwang, N. Murali, B. Mejia-Sosa, A. Lubarski, K. M. Teeluck, E. S. Hall, E. Garfunkel, M. Greenblatt, G. C. Dismukes, *Energy Environ. Sci.* **2018**, *11*, 2550.
[22] J. Lee, S. Kang, K. Yim, K. Kim, H. W. Jang, Y. Kang, S. Han, *J. Phys. Chem. Lett.* **2018**, *9*, 2049.
[23] H. Li, C. Tsai, A. L. Koh, L. Cai, A. W. Contryman, A. H. Fragapane, J. Zhao, H. S. Han, H. C. Manoharan, F. Abild-Pedersen, J. K. Nørskov, X. Zheng, *Nat. Mater.* **2016**, *15*, 48.
[24] D. Voiry, R. Fullon, J. Yang, C. de Carvalho Castro e Silva, R. Kappera, I. Bozkurt, D. Kaplan, M. J. Lagos, P. E. Batson, G. Gupta, A. D. Mohite, L. Dong, D. Er, V. B. Shenoy, T. Asefa, M. Chhowalla, *Nat. Mater.* **2016**, *15*, 1003.
[25] G. Li, D. Zhang, Q. Qiao, Y. Yu, D. Peterson, A. Zafar, R. Kumar, S. Curtarolo, F. Hunte, S. Shannon, Y. Zhu, W. Yang, L. Cao, *J. Am. Chem. Soc.* **2016**, *138*, 16632.
[26] H. P. Komsa, A. V. Krasheninnikov, *Phys. Rev. B* **2015**, *91*, 125304.
[27] J. Y. Noh, H. Kim, Y. S. Kim, *Phys. Rev. B* **2014**, *89*, 205417.
[28] J. K. Nørskov, J. Rossmeisl, A. Logadottir, L. Lindqvist, J. R. Kitchin, T. Bligaard, H. Jónsson, *J. Phys. Chem. B* **2004**, *108*, 17886.
[29] J. Rossmeisl, E. Skúlason, M. E. Björketun, V. Tripkovic, J. K. Nørskov, *Chem. Phys. Lett.* **2008**, *466*, 68.
[30] K. Y. Kim, J. Lee, S. Kang, Y. Kang, S. Han, *ACS Catal.* **2018**, *8*, 4508.
[31] Q. Lu, F. Jiao, *Nano Energy* **2016**, *29*, 439.
[32] C. Shi, H. A. Hansen, A. C. Lausche, J. K. Nørskov, *Phys. Chem. Chem. Phys.* **2014**, *16*, 4720.
[33] K. P. Kuhl, T. Hatsukade, E. R. Cave, D. N. Abram, J. Kibsgaard, T. F. Jaramillo, *J. Am. Chem. Soc.* **2014**, *136*, 14107.
[34] H. Xiao, T. Cheng, W. A. Goddard, R. Sundararaman, *J. Am. Chem. Soc.* **2016**, *138*, 483.
[35] A. A. Peterson, F. Abild-Pedersen, F. Studt, J. Rossmeisl, J. K. Nørskov, *Energy Environ. Sci.* **2010**, *3*, 1311.
[36] R. Kortlever, J. Shen, K. J. P. Schouten, F. Calle-Vallejo, M. T. M. Koper, *J. Phys. Chem. Lett.* **2015**, *6*, 4073.
[37] Z. W. Chen, W. Gao, W. T. Zheng, Q. Jiang, *ChemSusChem* **2018**, *11*, 1455.
[38] H. S. Sen, H. Sahin, F. M. Peeters, E. Durgun, *J. Appl. Phys.* **2014**, *116*, 083508.
[39] M. Karamad, H. A. Hansen, J. Rossmeisl, J. K. Nørskov, *ACS Catal.* **2015**, *5*, 4075.
[40] C. Genovese, C. Ampelli, S. Perathoner, G. Centi, *Green Chem.* **2017**, *19*, 2406.
[41] C. W. Kim, M. J. Kang, S. Ji, Y. S. Kang, *ACS Catal.* **2018**, *8*, 968.
[42] K. J. P. Schouten, Y. Kwon, C. J. M. van der Ham, Z. Qin, M. T. M. Koper, *Chem. Sci.* **2011**, *2*, 1902.
[43] J. H. Montoya, A. A. Peterson, J. K. Nørskov, *ChemCatChem* **2013**, *5*, 737.
[44] E. Tayyebi, J. Hussain, Y. Abghoui, E. Skúlason, *J. Phys. Chem. C* **2018**, *122*, 10078.
[45] M. Jouny, W. W. Luc, F. Jiao, *Ind. Eng. Chem. Res.* **2018**, *57*, 2165.
[46] X. Wang, Z. Li, J. Shi, H. Wu, Z. Jiang, W. Zhang, X. Song, Q. Ai, *ACS Catal.* **2014**, *4*, 962.
[47] C. A. Huff, M. S. Sanford, *J. Am. Chem. Soc.* **2011**, *133*, 18122.
[48] Y. Lum, J. W. Ager, *Energy Environ. Sci.* **2018**, *11*, 2935.
[49] S. Bontemps, L. Vendier, S. Sfabo-Etienne, *J. Am. Chem. Soc.* **2014**, *136*, 4419.
[50] K. Nakata, T. Ozaki, C. Terashima, A. Fujishima, Y. Einaga, *Angew. Chem. Int. Ed.* **2014**, *53*, 871; *Angew. Chem.* **2014**, *126*, 890.
[51] X. Hong, K. Chan, C. Tsai, J. K. Nørskov, *ACS Catal.* **2016**, *6*, 4428.
[52] G. Kresse, J. Furthmüller, *Phys. Rev. B* **1996**, *54*, 11169.
[53] J. P. Perdew, K. Burke, M. Ernzerhof, *Phys. Rev. Lett.* **1996**, *77*, 3865.
[54] S. Grimme, *J. Comput. Chem.* **2006**, *27*, 1787.
[55] K. Mathew, R. Sundararaman, K. Letchworth-Weaver, T. A. Arias, R. G. Hennig, *J. Chem. Phys.* **2014**, *140*, 084106.
[56] C. J. Camer, *Essentials of Computational Chemistry: Theories and Models*, John Wiley & Sons, Chichester, **2004**.
[57] H. Afeefy, J. Liebman, S. Stein in *NIST Chemistry WebBook, NIST Stand. Ref. Database Number 69* (Eds.: P. J. Linstrom, W. G. Mallard), National Institute of Standards and Technology, Gaithersburg, MD, **2018**, p. 20899.

Manuscript received: March 18, 2019
Revised manuscript received: April 20, 2019
Accepted manuscript online: April 25, 2019
Version of record online: May 24, 2019